Journal of Biomedical Optics

SPIEDigitalLibrary.org/jbo

Photoacoustic section imaging using an elliptical acoustic mirror and optical detection

Robert Nuster
Sibylle Gratt
Klaus Passler
Dirk Meyer
Guenther Paltauf

SPIE

Photoacoustic section imaging using an elliptical acoustic mirror and optical detection

Robert Nuster,[a] Sibylle Gratt,[a] Klaus Passler,[a] Dirk Meyer,[b] and Guenther Paltauf[a]
[a]Karl-Franzens University Graz, Department of Physics, 8010 Graz, Austria
[b]University of Innsbruck, Institute of Molecular Biology, 6020 Innsbruck, Austria

Abstract. A method is proposed that utilizes the advantages of optical ultrasound detection in two-dimensional photoacoustic section imaging, combining an optical interferometer with an acoustic mirror. The concave mirror has the shape of an elliptical cylinder and concentrates the acoustic wave generated around one focal line in the other one, where an optical beam probes the temporal evolution of acoustic pressure. This yields line projections of the acoustic sources at distances corresponding to the time of flight, which, after rotating the sample about an axis perpendicular to the optical detector, allows reconstruction of a section using the inverse Radon transform. A resolution of 120 μm within and 1.5 mm between the sections can be obtained with the setup. Compared to a bare optical probe beam, the signal-to-noise ratio (SNR) is seven times higher with the mirror. Furthermore, the imaging system is tested on a biological sample. © *2012 Society of Photo-Optical Instrumentation Engineers (SPIE).* [DOI: 10.1117/1.JBO.17.3.030503]

Keywords: photoacoustic imaging; section imaging; acoustic reflector; optical detection.

Paper 11655L received Nov. 7, 2011; revised manuscript received Jan. 11, 2012; accepted for publication Jan. 13, 2012; published online Mar. 2, 2012.

Photoacoustic (or optoacoustic) imaging (PAI) combines the favorable properties of diffuse optical imaging and ultrasound imaging, namely optical contrast with ultrasound spatial resolution. The contrast of the image is closely related to the distribution of light absorbing structures, such as blood vessels, and even to the oxygenation level of circulating blood. Promising medical applications are, for instance, small animal or human breast imaging.[1–6] The basic mechanism underlying PAI is the generation of sound waves due to thermal expansion of objects heated by light pulses (thermoelastic effect), which usually have a duration of the order of nanoseconds. After leaving the observed imaging volume, the sound waves are detected by broadband ultrasound sensors, and the recorded signals are used to reconstruct the distribution of initial pressure. This distribution is proportional to the absorbed energy density after the light pulse and is determined by the optical properties of the object.

For three-dimensional (3D) PAI, a standard method is to detect the sound waves with small, piezoelectric transducers, which are in the ideal case distributed on a closed surface surrounding the object. An alternative is the use of integrating line detectors, offering the possibility to choose from piezoelectric and various optical detection methods.[7–11] Unlike "point-like" detectors, the procedure to obtain the initial pressure distribution from line detector signals is a combination of back projection and the inverse Radon transform.[8,11]

Optical line detectors, such as a focused laser beam in an interferometer, combine high resolution (due to the small beam diameter and the high bandwidth of optical detection) and complete optical and acoustic transparency, leading to very accurate 3D images. However, when using a single integrating detector, it is very time-consuming to record the data, making the method ill-suited for *in vivo* experiments.

As a less time-consuming alternative to full 3D imaging, it is possible to restrict the imaging problem to a two-dimensional slice using cylindrically focusing elements.[12–14] With such elements, only pressure waves coming from a slab defined by the focal volume are detected. When small detector elements arranged around the object are used, the initial source can be recovered by back projecting the pressure signals over circles with the detector in the center. To improve the in-plane resolution, the effect of the finite size of the detector can be considered by deconvolution or iterative methods. Recently, cross-sectional imaging has been developed using a cylindrical, piezoelectric detector with a size larger than the imaging object. In that case, taking into account the integration of the pressure field over the extended detection area, the inverse Radon transform is used for the reconstruction.[9,15]

In this work, a method is proposed that combines the favorable properties of optical line detection with 2D section imaging. The heart of the imaging setup is an acoustic mirror having the shape of an elliptical cylinder. In one focal line of the mirror, the detection beam is located, whereas the sample is positioned in the other focal line. With this confocal arrangement, it is possible to probe the initial pressure distribution generated in the sample along part of the plane connecting the two focal lines. Due to the integrating property of line detector and mirror, the time dependent signals measured for a rotating sample are related to the Radon transform of the initial pressure in the imaging plane. Therefore, image reconstruction from the recorded signals requires only the application of the inverse Radon transform. Hence, this method is well suited for applications requiring fast and sensitive section imaging. The resolution and sensitivity of the detection system are investigated by experiments on phantom samples. Furthermore, the imaging system is tested on a biological sample.

The front and top views of the measurement setup are shown in Fig. 1. An elliptical cylinder with limited aperture (NA = 0.23) forms the acoustic mirror (AM). Its shape is given by the semi-major ($a = 30$ mm) and semi-minor ($b = 20$ mm) axes of the ellipse and its extension (60 mm) in y direction. In general, waves coming from one of the focal lines of the ellipse converge in the other one. An optical detection beam aligned along F1 probes at time $t = 2a/c_s$ (c_s is the speed of sound) the acoustic pressure coming from the initial pressure

Address all correspondence to: Robert Nuster, arl-Franzens University Graz, Department of Physics, 8010 Graz, Austria. Zip: 8010; Tel: 433163805195; E-mail: ro.nuster@uni-graz.at

0091-3286/2012/$25.00 © 2012 SPIE

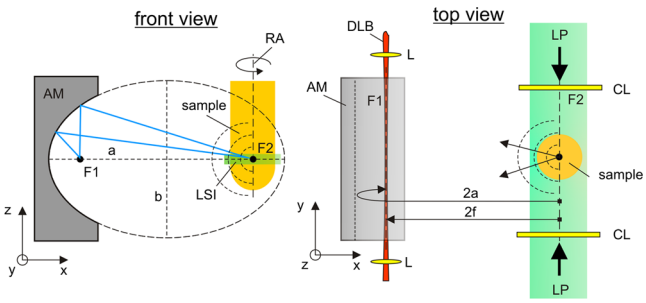

Fig. 1 Front and top view of the optical section imaging setup.

distribution integrated along the focal line F2. As a result of the finite aperture of the reflector (the fact that the ellipse is not closed), waves coming from lines parallel to F2 but at slightly offset x position will be concentrated at F1, though at a different time. This can be seen in analogy to a spherical lens with its finite depth of field as it is used in photoacoustic microscopy. In z direction, the sensitivity is still concentrated to a narrow range (Fig. 2). Hence, due to its focusing property, the setup is suitable for photoacoustic section imaging. Further narrowing of the sensitive volume in z direction can be obtained by line shaped illumination (LSI) of the sample from two opposite sides oriented in y direction. For this purpose, the setup is equipped with two cylindrical lenses (CL) shown in Fig. 1. For section imaging, the sample is rotated about an axis (RA) oriented in z direction. The axis crosses F2 in the center of the mirror with respect to its extension in y direction.

A detailed description of the integrating optical detection method can be found in Paltauf et al.[8] In brief, the pressure field is integrated along the focused detection laser beam (DLB) forming one branch of a Mach-Zehnder interferometer. Pressure variations cause a modulation of the refractive index of water via elasto-optic coupling. The resulting optical phase modulation is transformed into measurable intensity modulations by the interferometer and recorded with a balanced photodetector.

A measured time signal contains the unfocused acoustic wave arriving directly from the sample at the detection beam, as well as the acoustic wave coming from the reflector. To avoid an overlap of the acoustic signals, the maximum allowed diameter of the sample is limited to $D_{\max} = 2a - 2f$, where f is the distance from the center of the ellipse to the focal lines determined by $f = \sqrt{a^2 - b^2}$. Correspondingly, the upper limit of the sample diameter is 15 mm for the size of the used acoustic reflector. This device was designed for the imaging of zebra fish, which have typical diameters below this value.

To estimate the resolution in z direction, a spherical photoacoustic source with a diameter of 200 μm was used to probe the signal amplitude at different positions. For this purpose, the illumination was moved together with the sample to scan a rectangular range of 20 mm times 10 mm centered at F2. The increments in x and z directions were 400 μm and 300 μm, respectively. Figure 2 shows the measured signal amplitudes as a function of the position and an averaged profile in z direction. Since the full width half maximum value (FWHM) of the z profiles varies with distance to the focal line F2, we calculated the averaged z profile [Fig. 2(b)] over the full x range of 20 mm to estimate the z resolution. In this way, a value of 1.5 mm is obtained. This can be regarded as a worst case, since in an actual imaging experiment, the line shaped illumination would be fixed relative to the z position of F2, leading to some additional focusing on to the selected section of the object.

To demonstrate the experimental procedure and the properties of the measurement setup for section imaging, we used a well-defined sample. The phantom consisted of two spherical photoacoustic sources with diameters of 500 and 150 μm embedded in a gelatin matrix with a diameter of 10 mm. The line shaped illumination was fixed to the height of the focusing plane of the detector. Signals were acquired while rotating the

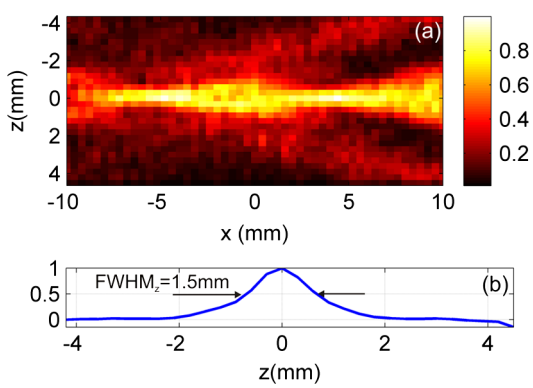

Fig. 2 (a) Dependence of the measured signal amplitude on the source position. The center of the image at $x = 0$ marks the position of the focal line F2. (b) Averaged z profile indicating the resolution between neighboring sections.

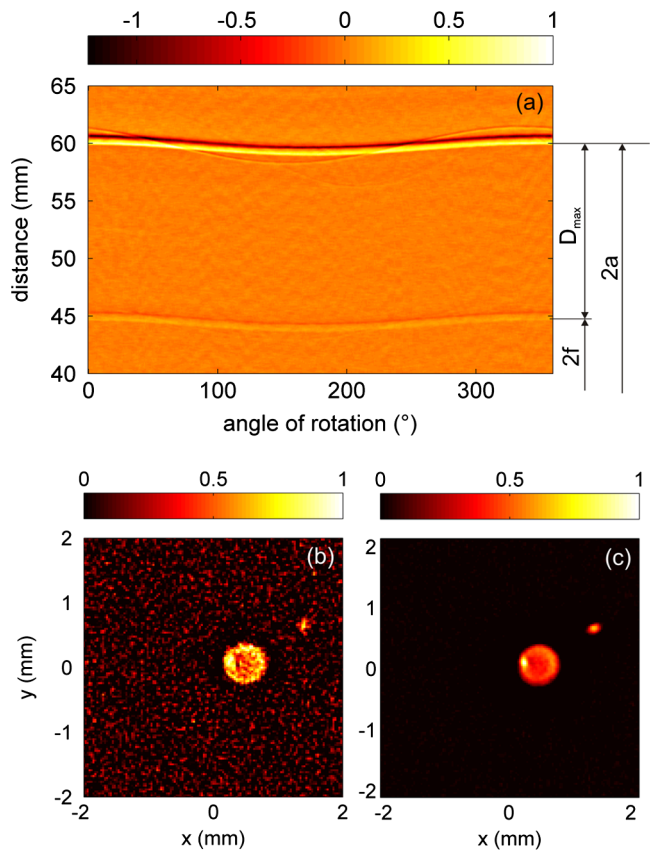

Fig. 3 (a) Recorded raw data showing the difference of the SNR of signals recorded with and without the influence of the acoustic mirror. (b) Image using the direct wave data. (c) Section image using the focused wave.

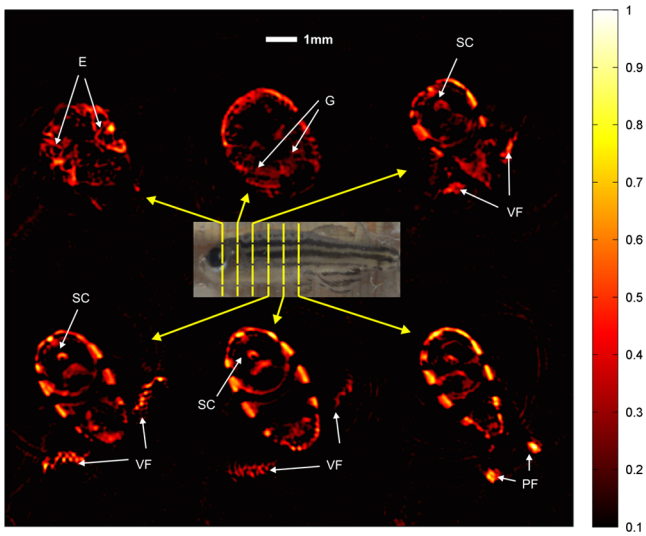

Fig. 4 Result of the section imaging experiment on a zebra fish. The step size between the sections was 2 mm: eyes (E), gill (G), spinal column (SC), ventral fins (VF), pelvic fins (PF).

sample over 360 deg with an angular increment of 0.9 deg without averaging. With the 10 Hz repetition rate of the pulsed laser, the data acquisition for a section image took 40 sec. The parameters for the rotation, the line shaped illumination, and the use of a 20 MHz bandwidth limitation of the storage oscilloscope during data acquisition were kept identical for all section imaging experiments shown in this work.

Figure 3(a) shows the recorded raw data from the circular scan at the z position containing the two spherical sources. The time axis is converted to distance by multiplication with the speed of sound of water. Sinusoidal structures are visible near 45 and 60 mm, indicating the direct, unfocused signals and the reflected signals, respectively. The distance between them is $D_{\max}$. Before reconstruction, the raw data were band pass filtered (200 kHz to 20 MHz) and Hilbert transformed. Finally, the inverse Radon transform was applied to each of the data sets to obtain the two section images shown in Figs. 3(b) and 3(c). A contrast to noise ratio (CNR) seven times higher is obtained in the image from the reflected data (with the AM) compared to the image from the direct signals. In the following experiments, we only evaluated the reflected signals.

The in-plane resolution (x-y plane) was estimated by sectional imaging of a black human hair with a diameter of 60 μm oriented in z direction. The cross-section of the hair appears with a diameter of 120 μm, which is a good estimate for the achievable resolution within the imaged sections. The discrepancy to the real dimension of the hair originates from the alignment accuracy of the acoustic mirror.

Finally, section images of a zebra fish are shown in Fig. 4. The fish was embedded in gelatine for stabilization and for fixing it on the rotational stage. For improvement of the CNR, the recorded temporal signals were averaged five times. In the images, the stripes, the eyes, the gill, the spine, the fins, and some other inner structures of the zebra fish can be distinguished. The sections were taken at a step size of 2 mm from the head to the tail, and one can see the location of the inner structures throughout the different sections.

In summary, a setup for photoacoustic section imaging is presented based on the combination of optical integrating detection with an acoustic reflector. The benefit of this combination is twofold. The elliptic acoustic reflector with its imaging properties enhances the sensitivity of the bare optical beam. The optical interferometric detector, in turn, provides accurate pressure signals due to its acoustic and optical transparency. Recording the data while rotating the sample over 360-deg section images can be obtained efficiently. Therefore, this method is ideally suited for imaging of selected slices of small animals in biological or preclinical research.

Acknowledgments

This work has been supported by the Austrian Science Fund (FWF), Project Nos. S10502-N20, S10508-N20, and S10509-N20.

References

1. M. H. Xu and L. V. Wang, "Photoacoustic imaging in biomedicine," *Rev. Sci. Instrum.* **77**(4), 041101 (2006).
2. P. Beard, "Biomedical photoacoustic imaging," *Interface Focus* **1**(4), 602–631 (2011).
3. J. Laufer et al., "Three-dimensional noninvasive imaging of the vasculature in the mouse brain using a high resolution photoacoustic scanner," *Appl. Opt.* **48**(10), D299–D306 (2009).
4. S. Manohar et al., "The Twente Photoacoustic Mammoscope: system overview and performance," *Phys. Med. Biol.* **50**(11), 2543–2557 (2005).
5. M. P. Fronheiser et al., "Real-time optoacoustic monitoring and three-dimensional mapping of a human arm vasculature," *J. Biomed. Opt.* **15**(2), 21305 (2010).
6. S. A. Ermilov et al., "Laser optoacoustic imaging system for detection of breast cancer," *J. Biomed. Opt.* **14**(2), 024007(2009).
7. R. Nuster et al., Comparison of optical and piezoelectric integrating line detectors, *Proc. SPIE* **7177**, 71770T (2009).
8. G. Paltauf et al., "Photoacoustic tomography using a Mach-Zehnder interferometer as acoustic line detector," *Appl. Opt.* **46**(16), 3352–3358 (2007).
9. P. Burgholzer et al., "Thermoacoustic tomography with integrating area and line detectors," *IEEE Trans. Ultrason. Ferroelectr. Freq. Control* **52**(9), 1577–1583 (2005).
10. H. Grün et al., "Three dimensional photoacoustic imaging using fiber-based line detectors," *J. Biomed. Opt.* **15**(2), 021306 (2010).
11. R. Nuster et al., "Photoacoustic microtomography using optical interferometric detection," *J. Biomed. Opt.* **15**(2), 021307 (2010).
12. X. D. Wang et al., "Noninvasive laser-induced photoacoustic tomography for structural and functional in vivo imaging of the brain," *Nat. Biotechnol.* **21**(7), 803–806 (2003).
13. J. Gamelin et al., "A real-time photoacoustic tomography system for small animals," *Opt. Express* **17**(13), 10489–10498 (2009).
14. D. Razansky et al., "Multispectral opto-acoustic tomography of deep-seated fluorescent proteins in vivo," *Nat. Photonics* **3**(7), 412–417 (2009).
15. S. Gratt et al., "Photoacoustic section imaging with an integrating cylindrical detector," *Biomed. Opt. Exp.* **2**(11), 2973–2981 (2011).